Magnon-driven chiral charge and spin pumping and electron-magnon scattering from time-dependent quantum transport combined with classical atomistic spin dynamics

Abhin Suresh,[1] Utkarsh Bajpai,[1] and Branislav K. Nikolić[1,2,*]

[1]*Department of Physics and Astronomy, University of Delaware, Newark, Delaware 19716, USA*

[2]*Kavli Institute for Theoretical Physics, University of California, Santa Barbara, California 93106-4030, USA*

(Received 1 April 2020; revised manuscript received 22 May 2020; accepted 26 May 2020; published 5 June 2020)

Using newly developed quantum-classical hybrid framework, we investigate interaction between spin-polarized conduction electrons and a single spin wave (SW) coherently excited within a metallic ferromagnetic nanowire. The SW is described by classical atomistic spin dynamics as a collection of precessing localized magnetic moments on each atom. The conduction electrons are described quantum mechanically using time-dependent nonequilibrium Green functions. When the nanowire hosting SW is attached to two normal metal (NM) leads, with no dc bias voltage applied between them, the SW pumps *chiral* electronic charge and spin currents into the leads. Their direction is tied to the direction of SW propagation and they scale linearly with the frequency of the precession. This is in contrast to standard pumping by the uniform precession mode with identical spin currents flowing in both directions and *no* accompanying charge current or experimentally observed [C. Ciccarelli *et al.*, Nat. Nanotechnol. **10**, 50 (2014); M. Evelt *et al.*, Phys. Rev. B **95**, 024408 (2017)] magnonic charge pumping which was interpreted by *requiring* spin-orbit (SO) coupling effects. Conversely, the mechanism behind our prediction is *nonadiabaticity due to time-retardation effects*—motion of localized magnetic moment affects conduction electron spin in a retarded way, so that it takes a finite time until the electron spin reacts to the motion of the classical vector. This makes the time-dependent nonequilibrium spin density misaligned with 'adiabatic direction,' even for zero SO coupling and in the absence of magnetic or spin-orbit impurities. We visualize retardation effects by computing the spatial profile of nonadiabaticity angle between the electronic nonequilibrium spin density and 'adiabatic direction.' Upon injecting dc spin-polarized charge current, electrons interact with SW where outflowing electronic charge and spin current are modified due to *both* scattering off time-dependent potential generated by the SW and superposition with the currents pumped by the SW itself. Using Lorentzian voltage pulse to excite leviton out of the Fermi sea, which carries one electron charge with no accompanying electron-hole pairs and behaves as solitonlike quasiparticle, we describe how a *single* electron interacts with a *single* SW.

DOI: 10.1103/PhysRevB.101.214412

I. INTRODUCTION

In the semiclassical picture [1,2], a spin wave (SW) is a disturbance in the local magnetic ordering of a ferromagnetic material in which localized magnetic moments precess around the easy axis with the phase of precession of adjacent moments varying harmonically in space over the wavelength λ, as illustrated in Fig. 1. The quanta of energy of SW behave as a quasiparticle, termed magnon, which carries energy $\hbar\omega$ and spin $\hbar$. The frequency ω of the precession is commonly in GHz range of microwaves, but it can reach THz range in antiferromagnets [3]. The SWs can be excited in equilibrium as incoherent thermal fluctuations, which then reduce the total magnetization with increasing temperature [4]. They can also be excited by external fields [5–10] which leads to coherent propagation of SWs as a dispersive signal.

Out of equilibrium, electron-magnon interaction is encountered in numerous phenomena in spintronic devices, such as inside magnetic layers or at their interfaces with layers of normal metals and insulators. For example, such processes can increase resistivity of ferromagnetic metal (FM) with temperature due to spin-flip scattering from thermal spin disorder [11,12], play an essential role in the laser-induced ultrafast demagnetization [13], generate nontrivial temperature and bias voltage dependence of tunneling magnetoresistance in magnetic tunnel junctions [14,15], open inelastic conducting channels [16], contribute to spin-transfer [17–19] and spin-orbit (SO) torques [20], and convert magnonic spin currents into electronic spin current or vice versa at magnetic-insulator/normal-metal interfaces [10,21–23]. Magnon driven *chiral* charge pumping—where magnon generates electronic charge current in the absence of any bias voltage, and with the direction of current changing upon reversing the direction of magnon propagation—has also been observed experimentally [7,24].

The nonequilibrium many-body perturbation theory [15,22], formulated using Feynman diagrams for nonequilibrium Green functions (NEGFs) [25], offers rigorous quantum-mechanical treatment of both electrons and magnons, once

*bnikolic@udel.edu

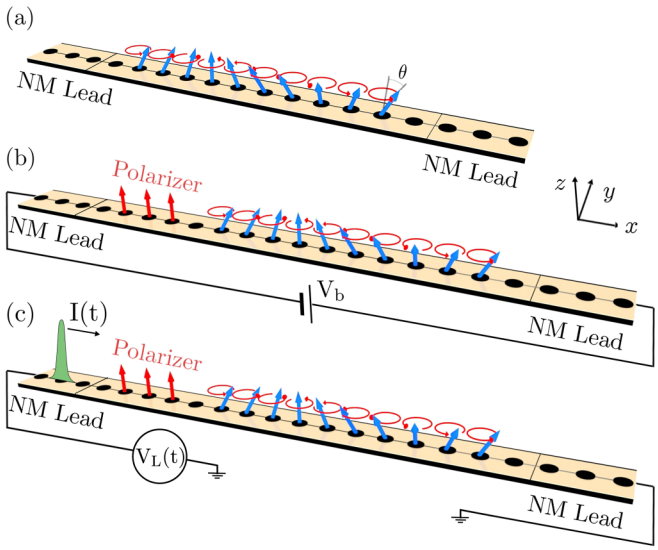

FIG. 1. Schematic view of two-terminal setups where FM wire, modeled as 1D chain of ferromagnetic atoms [29], hosts SW comprised of $N = 10$ localized magnetic moments $\mathbf{M}_i(t)$ precessing as classical vectors with frequency ω and cone angle $\theta = 10^\circ$ [6], as well as with harmonic variation in the phase of precession of adjacent moments. The wire is attached to the left and right semi-infinite normal metal leads which terminate into the macroscopic reservoirs wherein: (a) no bias voltage is applied between the reservoirs, (b) small bias voltage V_b is applied to inject dc unpolarized charge current into the wire, which is then spin polarized by three fixed spins (red arrows), and (c) Lorentzian voltage pulse [30,31] is applied between the reservoirs to inject leviton current pulse $I_L(t)$ into the wire carrying integer charge $Q = \int dt\, I_L(t) = 2e$.

the original spin operators are mapped to the bosonic ones [26]. However, to ensure current conservation, one has to sum large classes of such diagrams [27] which can lead to errors due to missed vertex corrections [28]. Furthermore, due to small magnon bandwidth, small electron-magnon interaction constant J_{sd} in the realm of electrons can become a strongly correlated regime for magnons due to large ratio J_{sd}/magnon-bandwidth. This can lead to quasibound states of magnons surrounded by electron-hole pairs [15], therefore suggesting that complicated higher order diagrams should be evaluated. This severely limits system size in two-terminal geometries of Fig. 1 or time scale over which electronic spin and charge currents, or magnonic spin current, can be computed. Since both electrons and magnons have intrinsic angular momentum, their translational flow leads to a flux of spin angular momentum as spin current.

On the other hand, experiments [5–8] exciting dipole or exchange dominated SWs are commonly interpreted using classical micromagnetics [1] or atomistic spin dynamics [2] simulations (the latter is akin to the former but with atomistic discretization). These methodologies describe SWs using trajectories of classical vectors $\mathbf{M}_i(t)$ of fixed (unit) length, pointing along the direction of localized magnetic moments or the corresponding localized spins, which precess around an easy axis with frequency ω and precession cone angle θ, as illustrated in Fig. 1. The cone angle has been measured [6] to be typically $\theta \lesssim 10^\circ$.

In this study, we employ recently developed multiscale and nonperturbative (i.e., numerically exact) time-dependent quantum transport combined with classical atomistic spin dynamics framework [32–35] to the problem of electron-SW interaction. This makes possible treating large number of time-dependent localized spins in experimentally relevant noncollinear configurations and over technologically relevant time scales $\sim$1 ns. The formalism combines time-dependent nonequilibrium Green function (TDNEGF) [25,36] description of electrons out of equilibrium in open quantum systems, such as those illustrated in Fig. 1, with the Landau-Lifshitz-Gilbert (LLG) equation describing classical dynamics of localized magnetic moments. The classical treatment of localized magnetic moments is justified [37] in the limit of large localized spins $S \to \infty$ and $\hbar \to 0$ (while $S \times \hbar \to 1$), as well as in the absence of entanglement [38] between the quantum state of localized spins which is expected to be satisfied at room temperature.

The paper is organized as follows. In Sec. II we introduce SW solution and its coupling to quantum Hamiltonian of electrons and TDNEGF calculations. Since explanation of electron-SW scattering for dc injected electronic current [Sec. III C] or leviton current pulse [Sec. III D] requires us to first understand how SW can pump spin and charge currents in the absence of any bias voltage, we carefully analyze the origin of such pumping in Sec. III A and Sec. III B, respectively. This includes computation of angles between the nonequilibrium electronic spin density, its 'adiabatic direction,' and localized magnetic moments which helps us to visualize time-retardation effects in Sec. III B. We conclude in Sec. IV.

II. MODELS AND METHODS

We assume that a single coherent SW has been excited externally, such as by microwave current flowing through narrow antennas [7]. Therefore, we fix dynamics of localized magnetic moment $\mathbf{M}_i(t)$ at site i of a one-dimensional (1D) lattice to be the SW solution [1,2] of the LLG equation (for simplicity without damping):

$$\mathrm{M}_i^x(t) = \sin\theta\, \cos(kx_i + \omega t), \tag{1a}$$

$$\mathrm{M}_i^y(t) = \sin\theta\, \sin(kx_i + \omega t), \tag{1b}$$

$$\mathrm{M}_i^z(t) = \cos\theta. \tag{1c}$$

Due to 1D geometry, the wave vector is just a number $k = 2\pi/[a(N-1)] = 2\pi/\lambda$, while the discrete coordinate is $x_i = (i-1)a$ and N is the total number of localized magnetic moments. Note that the *uniform mode*—which describes all magnetic moments precessing in-phase in magnetic materials driven by microwaves under the ferromagnetic resonance conditions [39]—is obtained by setting $k = 0$. Even though we employ 1D geometry as a tractable model of a realistic three-dimensional FM layer, such 1D geometries can even be realized experimentally as demonstrated by using an artificial chain of ferromagnetically coupled Fe atoms whose SWs were excited and detected using atom-resolved inelastic tunneling spectroscopy in a scanning tunneling microscope [29]. We note that the solution in Eq. (1) also appears in classical micromagnetics [1]. But there $\mathbf{M}_i$ represents magnetization of

a small volume of space, typically (2–10 nm)^3, rather than of individual atoms [2] that we must assume in order to couple classical dynamics of $\mathbf{M}_i(t)$ to time-dependent quantum transport calculations where electrons hop from atom to atom.

The FM nanowire hosting such SW is an *active region* of devices in Fig. 1, which is attached to two normal metal (NM) semi-infinite leads terminating into the macroscopic reservoirs. We use three different two-terminal geometries depicted Fig. 1: (a) No bias voltage V_b is applied between the left (L) and right (R) reservoirs kept at the same chemical potential $\mu_{\rm L} = \mu_{\rm R} = E_F$ where E_F is the Fermi energy in the Fermi function $f(E)$ of the reservoirs; (b) small dc bias voltage, $eV_b = \mu_{\rm L} - \mu_{\rm R} = 0.01$ eV, is applied between the reservoirs to inject unpolarized charge current into the active region where electrons are spin polarized by three static localized magnetic moments [red arrows in Fig. 1(b)] pointing along the z axis; (c) the Lorentzian voltage pulse [30,31] applied to the left NM lead injects a leviton current pulse $I_{\rm L}(t)$ carrying integer charge $Q = \int dt\, I_{\rm L}(t) = 2e$, which is then spin polarized by the same three static localized magnetic moments as in (b).

The quantum Hamiltonian of the electronic system within the FM nanowire is chosen as a 1D tight-binding model

$$\hat{H}(t) = -\sum_{\langle ij\rangle} \gamma_{ij} \hat{c}_i^\dagger \hat{c}_j - J_{sd} \sum_i \hat{c}_i^\dagger \boldsymbol{\sigma} \cdot \mathbf{M}_i(t) \hat{c}_i, \tag{2}$$

with an additional sd exchange interaction of strength $J_{sd} = 0.5$ eV [40] between $\mathbf{M}_i(t)$ from Eq. (1) and spin of the conduction electrons, described by the vector of the Pauli matrices $\boldsymbol{\sigma} = (\hat{\sigma}_x, \hat{\sigma}_y, \hat{\sigma}_z)$. Here $\hat{c}_i^\dagger = (\hat{c}_{i\uparrow}^\dagger \;\; \hat{c}_{i\downarrow}^\dagger)$ is a row vector containing operators $\hat{c}_{i\sigma}^\dagger$ which create an electron with spin $\sigma = \uparrow, \downarrow$ at site i, $\hat{c}_i$ is a column vector containing the corresponding annihilation operators, and $\gamma_{ij} = 1$ eV is the nearest-neighbor hopping. The NM leads are described by the same Hamiltonian as in Eq. (2) but with $J_{sd} \equiv 0$.

The fundamental quantity of nonequilibrium quantum statistical mechanics is the density matrix. The time-dependent one-particle density matrix can be expressed [36], $\boldsymbol{\rho}_{\rm neq}(t) = \mathbf{G}^<(t,t)/i$, in terms of the lesser GF of TDNEGF formalism defined by $G_{ii'}^{<,\sigma\sigma'}(t,t') = i\langle \hat{c}_{i'\sigma'}^\dagger(t') \hat{c}_{i\sigma}(t)\rangle$ where $\langle \ldots \rangle$ is the nonequilibrium statistical average [25]. We solve a matrix integro-differential equation [41]

$$i\hbar \frac{d\boldsymbol{\rho}_{\rm neq}}{dt} = [\mathbf{H}(t), \boldsymbol{\rho}_{\rm neq}] + i \sum_{p=L,R} [\boldsymbol{\Pi}_p(t) + \boldsymbol{\Pi}_p^\dagger(t)], \tag{3}$$

for the time evolution of the nonequilibrium density matrix $\boldsymbol{\rho}_{\rm neq}(t)$, where $\mathbf{H}(t)$ is the matrix representation of the Hamiltonian in Eq. (2). This can be viewed as an exact master equation for the reduced density matrix of the active region viewed as an open finite-size quantum system attached to macroscopic Fermi liquid reservoirs via semi-infinite NM leads. The leads ensure continuous energy spectrum of the system and, thereby, dissipation. The $\boldsymbol{\Pi}_p(t)$ matrices,

$$\boldsymbol{\Pi}_p(t) = \int_{t_0}^{t} dt_2 \, [\mathbf{G}^>(t,t_2)\boldsymbol{\Sigma}_p^<(t_2,t) - \mathbf{G}^<(t,t_2)\boldsymbol{\Sigma}_p^>(t_2,t)], \tag{4}$$

are expressed in terms of the lesser and greater GF and the corresponding self-energies $\boldsymbol{\Sigma}_p^{>,<}(t,t')$ [41]. They yield

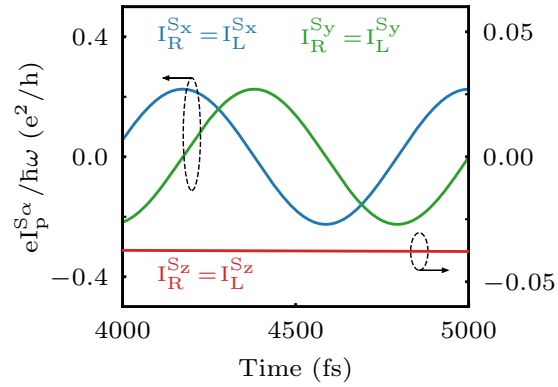

FIG. 2. Time dependence of electronic spin currents $I_{\rm L}^{S_\alpha}(t) = I_{\rm R}^{S_\alpha}(t)$ pumped symmetrically [39,43] into the left and right NM leads of setup in Fig. 1(a) whose localized magnetic moments precess as a uniform mode with $k = 0$ in Eq. (1). The Fermi energy is chosen as $E_F = -1.6$ eV, the frequency of precession is $\hbar\omega = 0.005$ eV, the total number of localized magnetic moments is $N = 10$ and dc bias voltage is *absent*, $V_b \equiv 0$.

directly time-dependent total charge current

$$I_p(t) = \frac{e}{\hbar} \mathrm{Tr}\,[\boldsymbol{\Pi}_p(t)], \tag{5}$$

and spin current

$$I_p^{S_\alpha}(t) = \frac{e}{\hbar} \mathrm{Tr}\,[\hat{\sigma}_\alpha \boldsymbol{\Pi}_p(t)], \tag{6}$$

flowing into the lead $p = {\rm L}, {\rm R}$. Local currents [42], or any other local quantity within the active region, are obtained by tracing the corresponding operator with $\boldsymbol{\rho}_{\rm neq}(t)$. We use the same units for charge and spin currents, defined as $I_p = I_p^\uparrow + I_p^\downarrow$ and $I_p^{S_\alpha} = I_p^\uparrow - I_p^\downarrow$, in terms of spin-resolved charge currents I_p^σ. In our convention, *positive* current in NM lead p means charge or spin is flowing *out* of that lead.

III. RESULTS

A. Spin-wave-driven chiral spin pumping

As a warm-up, we first consider standard [39,43–45] spin pumping by the uniform mode, with $k = 0$ in Eq. (1) and no dc bias voltage applied, which serves as a reference point for subsequent discussion. In this case, identical *pure* (i.e., not accompanied by any charge current) spin currents $I_{\rm L}^{S_\alpha}(t) = I_{\rm R}^{S_\alpha}(t)$ are pumped into both leads, as shown in Fig. 2. Their $I_{\rm L}^{S_z} = I_{\rm R}^{S_z}$ components are time independent, and their negative sign shows that they flow *into* the NM leads, as obtained also in the scattering theory [39], rotating frame approach [43] or Floquet-NEGF theory [44,45].

On the other hand, the excited SW in the setup of Fig. 1(a) pumps *both* charge and spin currents into the NM leads in the absence of any dc bias voltage. Their time dependences, $I_p^{S_\alpha}(t)$ and $I_p(t)$, are shown in Figs. 3(a)–3(c) after transient currents have died out. Furthermore, in contrast to pumping by the uniform mode, we find $|I_{\rm L}^{S_z}| > |I_{\rm R}^{S_z}|$. This is due to the spin current carried by the SW itself [10]. That is, spin current carried by the SW must be "transmuted" [46] into electronic spin current at the FM-wire/NM-left-lead interface [8,10,34] because no localized magnetic moments exist in

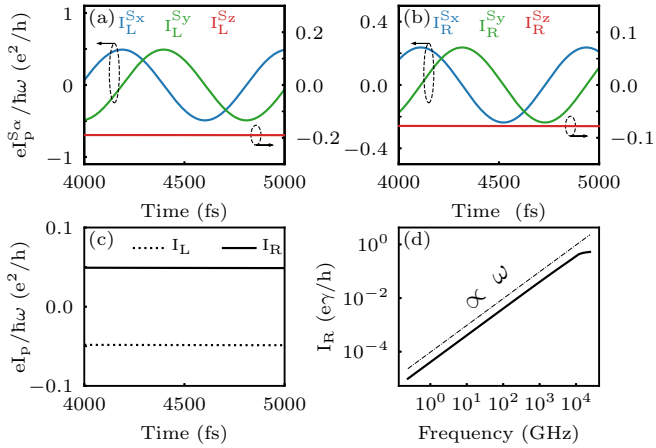

FIG. 3. Time dependence of electronic spin currents pumped into the (a) left and (b) right NM leads of setup in Fig. 1(a) whose localized magnetic moments precess as coherent SW mode with $k \neq 0$ in Eq. (1). (c) The SW with its nonuniform precessing magnetic moments also pumps dc charge current $I_L = -I_R$ into the NM leads, whose dependence on frequency (solid line) in panel (d) is linear $\propto\omega$ (dash-dot line). The Fermi energy is chosen as $E_F = -1.6$ eV, the frequency of SW is $\hbar\omega = 0.005$ eV, the total number of localized magnetic moments is $N = 10$ and dc bias voltage is *absent*, $V_b \equiv 0$.

the NM lead to support transport of angular momentum via their dynamics. This current is then added or subtracted to symmetrically pumped spin currents into the left or right NM leads, respectively. This explanation is supported by the fact that changing the sign of k in Eq. (1) leads to a reversed situation, $|I_L^{S_z}| < |I_R^{S_z}|$.

B. Spin-wave-driven chiral charge pumping

The charge pumping in spintronic devices with excited coherent SWs was observed experimentally in compressively strained (Ga,Mn)As bar [24], as well as in YIG/graphene heterostructures [7]. In the latter case, SW is excited within insulating YIG while pumped current flows through metallic graphene where localized magnetic moments are induced by the magnetic proximity effect [47]. The charge current pumped by time-dependent noncoplanar and noncollinear magnetic texture, described by local magnetization $\mathbf{m}(\mathbf{r}, t)$ as a continuous variable,

$$j_\alpha(\mathbf{r}) = C[\partial_\alpha \mathbf{m}(\mathbf{r}, t) \times \mathbf{m}(\mathbf{r}, t)] \cdot \partial_t \mathbf{m}(\mathbf{r}, t), \tag{7}$$

is the subject of the spin motive force (SMF) theory [48–53]. Equation (7), which is rooted in the associated geometrical (or Berry) phase [56], is valid when electron spins can follow "adiabatically" [54,55] the instantaneous configuration of $\mathbf{M}_i(t)$, which requires $J_{sd} \gg \hbar|\partial_t \mathbf{m}|$, $\hbar v_F |\partial_\alpha \mathbf{m}|$ (v_F is the Fermi velocity). In Eq. (7), we use notation $\partial_t = \partial/\partial t$ and $\partial_\alpha = \partial/\partial\alpha$ for $\alpha \in \{x, y, z\}$, $C = PG_0\hbar/2e$ is constant with proper units, $P = (G^\uparrow - G^\downarrow)/(G^\uparrow + G^\downarrow)$ is the spin polarization of the ferromagnet, and $G_0 = G^\uparrow + G^\downarrow$ is the total conductivity.

If we plug the SW solution for the local magnetization—$m_x(x) = \sin\theta\cos(kx + \omega t)$, $m_y(x) = \sin\theta\sin(kx + \omega t)$, and $m_z(x) = \cos\theta$—into Eq. (7) we obtain *zero* pumped charge current, $j_x(x) \equiv 0$. It is worth mentioning that plugging in the SW solution from Eq. (1) into the discretized version of Eq. (7)

$$j_x(i) = \frac{C}{a}[\partial_t \mathbf{M}_i \times \mathbf{M}_{i+1}] \cdot \mathbf{M}_i, \tag{8}$$

apparently leads to a nonzero result, $j_x(i) = \frac{C\omega}{a}\sin\theta\sin 2\theta\sin^2(ka/2)$ which contradicts $j_x(x) \equiv 0$ obtained from the continuous formula in Eq. (7). But in the limit of lattice spacing going to zero, $a \to 0$, we use $\lim_{a\to 0}\frac{1}{a}\sin^2(ka/2) = 0$ to arrive at the same conclusion, $j_x(i) \equiv 0$.

Thus, to explain nonzero charge pumping by SW in Ref. [7], a modified version of the SMF formula in Eq. (7) was employed which includes the so-called β term [51,52,56] due to nonadiabaticity

$$j_\alpha(\mathbf{r}) = C[\partial_\alpha \mathbf{m}(\mathbf{r}, t) \times \mathbf{m}(\mathbf{r}, t) + \beta\partial_\alpha \mathbf{m}(\mathbf{r}, t)] \cdot \partial_t \mathbf{m}(\mathbf{r}, t). \tag{9}$$

The β term is standardly justified by spin relaxation processes due to magnetic or SO impurities [57], which cause misalignment between electron spin and its perfectly 'adiabatic direction' tracking the instantaneous configuration of $\mathbf{M}_i(t)$. In the case of Dirac materials like graphene, with intrinsic or proximity SO coupling in its band structure (which YIG can induced in graphene via screw dislocation and a torsion of its honeycomb lattice [7]), even *spin-independent impurities* can cause spin relaxation [58]. This requires that equilibrium spin texture is tilted out of the plane (such as by spin-valley coupling) [58,59]. Using the SW solution from Eq. (1) in the discretized version of the β term in Eq. (9) gives

$$j_x^\beta(i) = C\beta\partial_t \mathbf{M}_i \cdot \left(\frac{\mathbf{M}_{i+1} - \mathbf{M}_i}{a}\right)$$
$$= C\beta\omega\sin^2\theta\left(\frac{\sin ka}{a}\right) \xrightarrow[a\to 0]{} Ck\omega\sin^2\theta. \tag{10}$$

The final result explains the experimentally observed [7] chiral nature of pumping where charge current changes sign upon $k \to -k$.

Figure 4 compares analytical result from Eq. (10) (dashed line) with the one from our TDNEGF calculations (solid line).

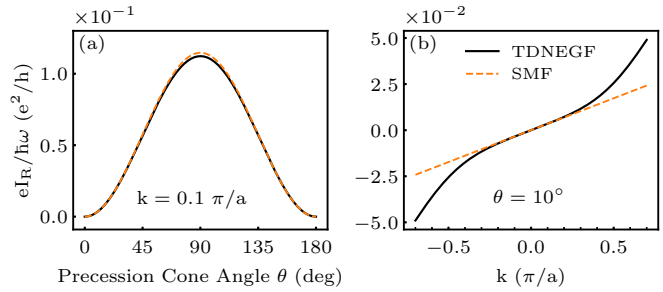

FIG. 4. The dependence of charge current from Fig. 3(c) on: (a) precession cone angle θ and (b) wave vector k of the SW. The solid lines are obtained from TDNEGF calculations and the dashed line is obtained from the β term in Eqs. (9) and (10) which corrects [51,52] the original SMF formula in Eq. (7) in order to take into account nonadiabatic effects [56,57].

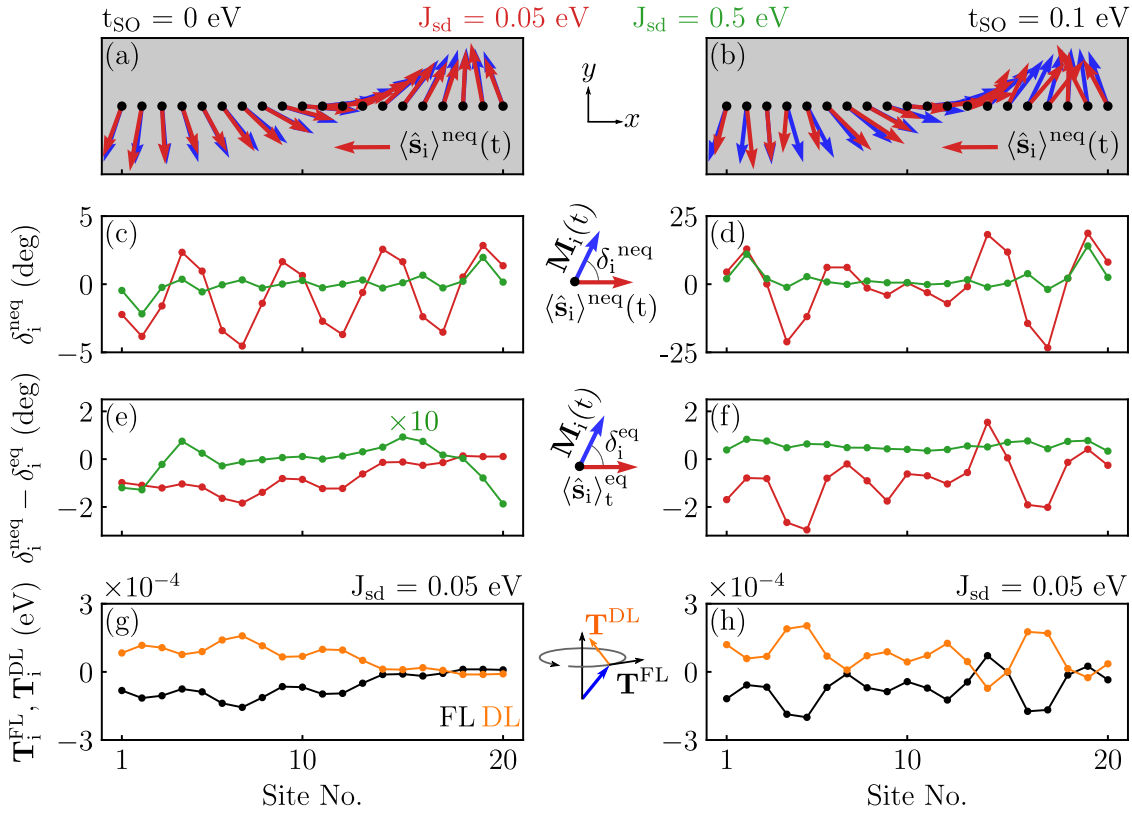

FIG. 5. (a),(b) Spatial profile at time $t = 2\pi/\omega$ of the in-xy-plane component of nonequilibrium electronic spin density vector $\langle\hat{\mathbf{s}}_i\rangle^{\text{neq}}(t)$ [Eq. (11)] and localized magnetic moments $\mathbf{M}_i(t)$ across FM nanowire hosting a SW of wave vector $k = 0.2\pi/a$. (c),(d) Spatial profile of angle δ_i^{neq}, illustrated in the inset between panels (c) and (d), between vectors of the nonequilibrium spin density $\langle\hat{\mathbf{s}}_i\rangle^{\text{neq}}(t)$ and classical localized magnetic moment $\mathbf{M}_i(t)$. (e),(f) Spatial profile of *nonadiabaticity angle*, $\delta_i^{\text{neq}} - \delta_i^{\text{eq}}$, between $\langle\hat{\mathbf{s}}_i\rangle^{\text{neq}}(t)$ and adiabatic spin density $\langle\hat{\mathbf{s}}_i\rangle_t^{\text{eq}}$ [Eq. (13)]. (g),(h) Spatial profile of FL and DL components of STT [Eq. (14)], illustrated in the inset between panels (g) and (h), exerted on $\mathbf{M}_i(t)$ at time $t = 2\pi/\omega$ due to nonzero angle $\delta_i^{\text{neq}} - \delta_i^{\text{eq}}$. In panels (a),(c),(e),(g) SO coupling is absent, while in panels (b),(d),(f),(h) we use the Rashba SO coupling [Eq. (12)] of strength $t_{\text{SO}} = 0.1$ eV. Two different values of *sd* exchange interaction in the Hamiltonian [Eq. (2)] are used, $J_{\text{sd}} = 0.05$ eV (red lines) and $J_{\text{sd}} = 0.5$ eV (green lines). The Fermi energy is chosen as $E_F = -1.6$ eV, the frequency of SW is $\hbar\omega = 0.005$ eV, the total number of localized magnetic moments is $N = 20$, and dc bias voltage is absent, $V_b \equiv 0$.

They closely follow each other [Fig. 4(a)] as a function of cone angle θ, except around $\theta = 90^\circ$, as well as as a function of k [Fig. 4(b)] within $|k| \lesssim 0.2\pi/a$ interval. Since our TDNEGF calculations are numerically exact, such deviations (for values of θ and k not commonly found in experiments though [6,8]) stem from the fact that the SMF formula in Eq. (9) contains only the lowest order [50,51] time and spatial derivatives of local magnetization.

At first sight, it seems surprising that we reproduce (within some interval) Eq. (10) even though our setup in Fig. 1(b) *does not contain* obvious sources of nonzero β, such as impurities or SO coupling in the band structure [57]. To clarify this, we compute electronic nonequilibrium spin density at site i

$$\langle\hat{\mathbf{s}}_i\rangle^{\text{neq}}(t) = \frac{\hbar}{2}\text{Tr}\left[\boldsymbol{\rho}_{\text{neq}}(t)|i\rangle\langle i|\otimes\boldsymbol{\sigma}\right], \tag{11}$$

and plot [Figs. 5(a)–5(d)] spatial profile (at fixed time $t = 2\pi/\omega$) of angle δ_i^{neq} [see inset between Figs. 5(c) and 5(d)] between $\langle\hat{\mathbf{s}}_i\rangle^{\text{neq}}(t)$ and $\mathbf{M}_i(t)$ across the whole chain with an excited SW. This angle is nonzero in Figs. 5(a) and 5(c) in the absence of SO coupling or spin-dependent impurities, and it increases in Figs. 5(b) and 5(d) after the Rashba SO coupling [60],

$$\hat{H}_{\text{SO}} = \sum_{ij}\hat{c}_i^\dagger\mathbf{t}_{ij}\hat{c}_j, \tag{12}$$

is added into the quantum Hamiltonian in Eq. (2). Here $\mathbf{t}_{ij} = -it_{\text{SO}}\hat{\sigma}_y$ for $i = j+1$. The strength of the Rashba SO coupling is chosen as $t_{\text{SO}} = 0.1$ eV, which generates conventional static Gilbert damping $\alpha_{\text{G}} = 0.01$ via the scattering theory [61] as the typical value [62] found in FM nanowires.

In addition, we examine instantaneous equilibrium spin density

$$\langle\hat{\mathbf{s}}_i\rangle_t^{\text{eq}} = \frac{\hbar}{2}\text{Tr}\left[\boldsymbol{\rho}_t^{\text{eq}}|i\rangle\langle i|\otimes\boldsymbol{\sigma}\right], \tag{13}$$

which is obtained from the equilibrium density matrix [25], $\boldsymbol{\rho}_t^{\text{eq}} = -\frac{1}{\pi}\int_{-\infty}^{+\infty} dE\,\text{Im}\,\mathbf{G}_t(E)f(E)$ using the frozen (adiabatic) retarded Green function, $\mathbf{G}_t(E) = [E - \mathbf{H}_t - \boldsymbol{\Sigma}]^{-1}$, computed for instantaneous configuration of $\mathbf{M}_i(t)$. Here we use subscript t to emphasize *parametric dependence* on time through slow variation of $\mathbf{M}_i(t)$, and $\boldsymbol{\Sigma} = \boldsymbol{\Sigma}_{\text{L}} + \boldsymbol{\Sigma}_{\text{R}}$ is the sum of the retarded self-energies of the leads. Thus, $\langle\hat{\mathbf{s}}_i\rangle_t^{\text{eq}}$ rigorously defines the meaning of 'adiabatic direction'

[51,52,56] for electronic spins. Its derivation assumes $d\mathbf{M}_i/dt \to 0$. For example, first nonadiabatic correction, that depends linearly on $d\mathbf{M}_i/dt$ and parametrically on time through $\mathbf{M}_i(t)$, can be derived [63,64] from $\mathbf{G}^<(t,t)$ by expanding it into a power series in the small parameter $d\mathbf{M}_i/dt$ and by retaining only the first order. Note that our numerically exact $\mathbf{G}^<(t,t)$ employed to obtain $\langle\hat{\mathbf{s}}_i\rangle^{\rm neq}(t)$ in Eq. (11) effectively includes all orders of such series. In the case of the dynamics of a single localized magnetic moment [55], and in the adiabatic limit $J_{sd}/\hbar\omega \gg 1$, $\langle\hat{\mathbf{s}}_1\rangle_t^{\rm eq} \parallel \mathbf{M}_1(t)$ and angle $\delta_1^{\rm eq} = 0$. However, the angle $\delta_i^{\rm eq}$ [see inset between Figs. 5(e) and 5(f)] between $\langle\hat{\mathbf{s}}_i\rangle_t^{\rm eq}$ and $\mathbf{M}_i(t)$ is not zero in any noncollinear configurations of $\mathbf{M}_i(t)$.

The adiabaticity assumption [51,52,54,56], according to which electronic quantum state follows the instantaneous SW configuration in the limit $J_{sd}/\hbar\omega \gg 1$, would imply that $\langle\hat{\mathbf{s}}_i\rangle^{\rm neq}(t)$ remains parallel to $\langle\hat{\mathbf{s}}_i\rangle_t^{\rm eq}$. In contrast, spatial profile of *nonadiabaticity angle*, $\delta_i^{\rm neq} - \delta_i^{\rm eq}$, plotted in Fig. 5(e) in the absence of SOC and in Fig. 5(f) in the presence of the Rashba SOC, demonstrates that $\langle\hat{\mathbf{s}}_i\rangle^{\rm neq}(t)$ is *not parallel* to $\langle\hat{\mathbf{s}}_i\rangle_t^{\rm eq}$, even in the perfectly justified adiabatic limit $J_{sd}/\hbar\omega = 100$ (green lines in Fig. 5). The nonadiabaticity angle $\delta_i^{\rm neq} - \delta_i^{\rm eq}$ visualized in Figs. 5(e) and 5(f) decreases with increasing $J_{sd}/\hbar\omega$, but making $(\delta_i^{\rm neq} - \delta_i^{\rm eq}) \to 0$ would require unrealistically large J_{sd}—the realistic values measured experimentally are $J_{sd} \simeq 0.1$ eV [40].

Thus, difference [32] $\langle\hat{\mathbf{s}}_i\rangle^{\rm neq}(t) - \langle\hat{\mathbf{s}}_i\rangle_t^{\rm eq}$ and its noncollinearity with $\mathbf{M}_i$ generates spin-transfer torque (STT) [65] on localized magnetic moment at site i

$$\mathbf{T}_i(t) = J_{sd}\left[\langle\hat{\mathbf{s}}_i\rangle^{\rm neq}(t) - \langle\hat{\mathbf{s}}_i\rangle_t^{\rm eq}\right] \times \mathbf{M}_i(t) = \mathbf{T}_i^{\rm DL}(t) + \mathbf{T}_i^{\rm FL}(t). \tag{14}$$

As usual [65], we split the STT vector [as illustrated in the inset between Fig. 5(g) and Fig. 5(h)] into two components: even under time-reversal or fieldlike (FL) torque, that affects precession around the easy axis, and odd under time reversal or dampinglike (DL) torque, which either enhances the Gilbert damping by pushing magnetic moment toward the axis of precession or competes with it as "antidamping." For example, negative value of $T_i^{\rm DL} = \mathbf{T}_i^{\rm DL} \cdot \mathbf{e}_{\rm DL}$ in Figs. 5(g) and 5(h), where $\mathbf{e}_{\rm DL}$ is the unit vector in the direction of $\mathbf{M}_i \times \partial\mathbf{M}_i/\partial t$, means that $\mathbf{T}_i^{\rm DL}$ vector points away from the easy axis which is "antidamping" action. Similarly, $T_i^{\rm FL} = \mathbf{T}_i^{\rm FL} \cdot \mathbf{e}_{\rm FL}$, where $\mathbf{e}_{\rm FL}$ is the unit vector in the direction of $\partial\mathbf{M}_i/\partial t$, is plotted in Figs. 5(g) and 5(h). In the absence of SO coupling $\mathbf{T}_i^{\rm DL}$ points toward the easy axis at all sites i in Fig. 5(g), which is time-dependent contribution to damping discussed in more details in Refs. [33,66,67]. Note, however, that we fix the dynamics of localized magnetic moments to SW solutions in Eq. (1), rather than solving TDNEGF and LLG equations self-consistently as performed in Refs. [32–34]. In the presence of the Rashba SO coupling, $\mathbf{T}_i^{\rm DL}$ can change sign, thereby acting as both damping and antidamping torque depending on the site i in Fig. 5(h).

Thus, TDNEGF calculations naturally include additional sources of nonadiabaticity for quantum dynamics of electronic spins and damping for classical dynamics of localized magnetic moments. They are operative even when SO coupling in the band structure is zero and spin-dependent impurities are absent, which is traditionally considered as necessary for nonadiabaticity or damping [56,57]. These effects stem from the fact that $\langle\hat{\mathbf{s}}_i\rangle^{\rm neq}(t)$ is always somewhat behind 'adiabatic direction' set by $\langle\hat{\mathbf{s}}_i\rangle_t^{\rm eq}$ because classical magnetization affects the conduction electrons in a *retarded way* [33,66]. That is, it always takes a finite amount of time until the conduction electron spin $\langle\hat{\mathbf{s}}_i\rangle^{\rm neq}(t)$ reacts to the motion of $\mathbf{M}_i(t)$. Similar magnitude of $\mathbf{T}_i^{\rm DL}$ torque component in Fig. 5(h) with *zero* SO coupling and Fig. 5(h) with *nonzero* SO coupling shows that retardation effects are an equally important physical mechanism of (time-dependent [33,66,67]) Gilbert damping as is traditionally considered SO coupling combined with electron-phonon interactions [68,69].

An alternative way to interpret the origin of charge pumping by SW is to analyze its frequency dependence shown in Fig. 3(d). This complies with the general theory of "adiabatic" quantum pumping [42,70,71] since it scales linearly with frequency in the physically relevant frequency range GHz–THz [3]. Note that terminology "adiabatic" in this context is not related to spin—instead it signifies sufficiently slow change of harmonic potential driving the quantum system so that its frequency is $\hbar\omega \ll E_F$ and/or smaller than relevant relaxation time for orbital dynamics of electrons. We recall that such linear scaling is in accord with the key requirement—*breaking of left-right symmetry*—for nonzero dc component of quantum charge pumping by a time-dependent potential [42,70,71]. This can be achieved by breaking inversion symmetry and/or time-reversal symmetry. In the "adiabatic" regime, quantum charge pumping requires both inversion and time-reversal symmetries to be broken dynamically, such as by two spatially separated potentials oscillating out-of-phase [70], which leads to $\bar{I}_p(t) \propto \omega$ at low frequencies ($\bar{A}$ is the average of quantity A over one period). In the case of SW, it is the wavelike pattern of precessing localized magnetic moments which dynamically breaks the left-right symmetry in Fig. 1(a), with respect to the vertical plane positioned between moments localized at sites $i = N/2$ and $i = N/2 + 1$. In contrast, in the "nonadiabatic" regime only one of those two symmetries needs to be broken and this does not have to occur dynamically. The dc component of the pumped current in the "nonadiabatic" regime is [71] $\bar{I}_p(t) \propto \omega^2$ at low frequencies as obtained in, e.g., the case of charge pumping by uniform mode across potential barrier that breaks the left-right symmetry of the device statically [43].

C. Electron/spin-wave scattering for injected dc spin-polarized charge current

For the setup in Fig. 1(b), we first establish (after some transient period not shown explicitly) steady charge current $I_{\rm R}$ [flat line in Fig. 6(c) for $t < 500$ fs] of electrons injected by dc bias voltage into $3 + 10$ static localized magnetic moments oriented along the z axis. The initially unpolarized current becomes spin polarized due to static moments, as characterized by steady spin current $I_{\rm R}^{S_z} \neq 0$ [flat line in Fig. 6(b) for $t < 500$ fs] and the corresponding spin polarization $P_z = |I_{\rm R}^{S_z}|/|I_{\rm R}| \approx 50\%$. Then at $t = 500$ fs we *suddenly* excite SW composed of 10 precessing localized magnetic moments in Fig. 1(b). This induces transient currents around that instant

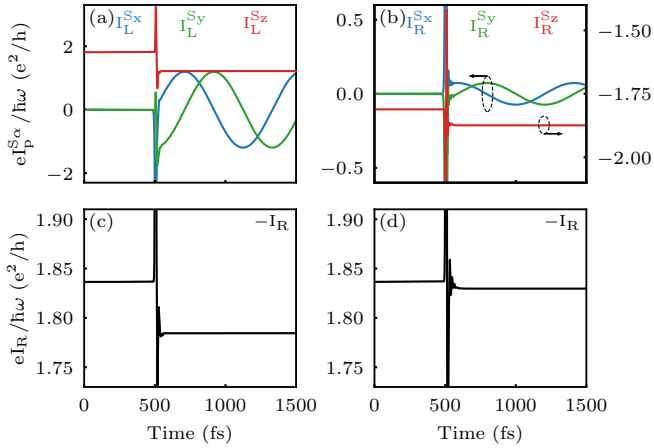

FIG. 6. Time dependence of electronic spin currents in the (a) left and (b) right NM leads of setup in Fig. 1(b) whose localized magnetic moments start to precess at $t = 500$ fs as a coherent SW with $k \neq 0$ in Eq. (1) in the presence of a flux of electrons injected into the active region by dc bias voltage $eV_b = 0.01$ eV. The electrons are spin polarized by three fixed spins (red arrows) in Fig. 1(b). The corresponding time dependence of their charge current $I_R(t)$ is shown in panel (c). Panel (d) plots time dependence of $I_R(t)$ for "frozen-in-time" [12] SW where $t = 0$ in Eq. (1). The Fermi energy is chosen as $E_F = -1.6$ eV, the frequency of SW is $\hbar\omega = 0.005$ eV, the total number of localized magnetic moments is $N = 10$, and dc bias voltage is $V_b = 0.01$ V.

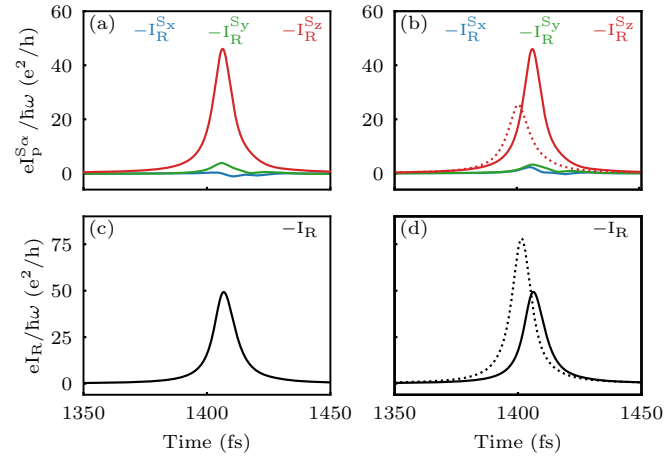

FIG. 7. Time dependence of electronic spin currents $I_R^{S_\alpha}(t)$ in the right NM lead after unpolarized leviton is injected by the Lorentzian voltage pulse [30,31] into the active region hosting: (a) three static localized magnetic moments (red arrows) pointing along the z axis, acting as spin polarizer, followed by SW excited at $t = 500$ fs, as illustrated in Fig. 1(c); (b) three static localized magnetic moments and a "frozen-in-time" SW excited at $t = 500$ fs. Panels (c) and (d) show time dependence of the charge current $I_R(t)$ corresponding to (a) and (b), respectively. In addition, panels (b) and (d) plot (dotted lines) time dependence of $I_R^{S_\alpha}(t)$ and $I_R(t)$, respectively, for the active region containing only the three static localized magnetic moments pointing along the z axis. The Fermi energy is chosen as $E_F = -1.6$ eV, the frequency of SW is $\hbar\omega = 0.005$ eV, and the total number of localized magnetic moments is $N = 10$.

which help us to visualize the boundary between the time interval without and with SW being present. Within the time interval $t > 500$ fs where SW is present, new time-dependent spin currents $I_p^{S_x}(t)$ and $I_p^{S_y}(t)$ emerge [Figs. 6(a) and 6(b)] due to spin pumping by SW demonstrated in Figs. 3(a) and 3(b).

Concurrently, dc spin currents $I_L^{S_z}$ [Fig. 6(a)] and $I_R^{S_z}$ [Fig. 6(b)], as well as dc charge current I_R [Fig. 6(c)], are reduced compared to their values prior to SW excitation. This reduction is mostly due to charge and spin currents pumped in the direction right-NM-lead→left-NM-lead in Fig. 3, which is opposite to the flow of originally injected charge and spin currents by dc bias voltage. Thus, outflowing spin and charge currents in the right NM lead can also be enhanced if we invert the sign of k in Eq. (1) and, therefore, the direction of SW propagation. Another reason for the reduction is backscattering of electrons by time-dependent potential generated by SW. The magnitude of reduction due to backscattering for charge current shown in Fig. 6(c) is estimated using $[I_R(t < 500\text{ fs}) - I_R(t > 500\text{ fs}) + I_R^{SW}]/I_R(t < 500\text{ fs}) \simeq 1\%$. Here I_R^{SW} denotes charge current pumped by SW [Fig. 3(c)] in the absence of any dc bias voltage V_b.

Recent *time-independent* quantum transport calculations [12] of the resistance of FM layers have included "frozen magnons" as correlated spin disorder where localized spins are tilted away from the easy axis in accord with thermal population of magnon modes. To understand time-dependent effects missed in such calculations, we freeze localized magnetic moments by setting $t = 0$ in Eq. (1). The scattering from such "frozen-in-time" SW leads to much smaller current reduction in Fig. 6(d).

D. Electron/spin-wave scattering for injected spin-polarized charge current leviton pulse

In order to simulate single-electron/single-SW scattering, we inject pulsed current into the active region using the Lorentzian voltage pulse [41], $V_L(t) = 2\hbar\tau/[(t-t_0)^2 + \tau^2]$, where the pulse duration is $\tau = 7.5\hbar/\gamma$. As confirmed experimentally [72], such special pulse profile with $\frac{e}{\hbar}\int dt\, V_L(t) = 2\pi n$ [73] drives the Fermi sea in the left reservoir to ensure [30,31] excitation of an integer number n of purely electronic states above the sea. They appear without spurious electron-hole pairs and exhibit minimal [74] nonequilibrium noise in charge transfer across the active region. We use $n = 2$, so that injected unpolarized charge current pulse, called leviton [72], carries charge $Q = \int dt\, I_L(t) = 2e$. This can be viewed as minimalistic unpolarized current composed of one spin-↑ and one spin-↓ electron flowing together. Upon spin polarization by three static localized magnetic moments in Fig. 1(c), the leviton interacts with SW excited suddenly at $t = 500$ fs. After such interaction, leviton outflows into the right NM lead where its spin and charge currents are plotted in Figs. 7(a) and 7(c), respectively. For comparison, Figs. 7(b) and 7(d) plot spin and charge currents in the right NM lead, respectively, for a leviton interacting with "frozen-in-time" SW. In addition, Figs. 7(b) and 7(d) also include (dotted lines) spin and charge current of leviton outflowing into the right NM lead when SW in Fig. 1(c) is removed from the active region. The integrals for outflowing spin-polarized leviton after scattering from SW in Figs. 7(a) and 7(c) are $\int dt\, I_R^{S_z}(t) = 0.939e$ and

$\int dt\, I_{\rm R}(t) = 0.822e$, respectively. They can be compared to $\int dt\, I_{\rm R}^{S_z}(t) = 0.944e$ and $\int dt\, I_{\rm R}(t) = 0.827e$ in Figs. 7(b) and 7(d), respectively. Note that the ratio of integrals of two dotted curves in Figs. 7(b) and 7(d) is $P_z = |\int dt\, I_{\rm R}^{S_z}(t)|/|\int dt\, I_{\rm R}(t)| \approx 40\%$ which can be considered as the spin polarization of leviton after passing through three static localized magnetic moments in Fig. 1(c).

IV. CONCLUSIONS

In conclusion, using time-dependent quantum transport combined with classical atomistic spin dynamics multiscale framework [32–34] we predict that SW coherently excited within a metallic ferromagnet will pump *chiral* electronic charge and spin currents into the attached normal metal leads. The chirality of pumped currents means that their direction is tied to the direction of SW propagation, changing upon reversal of the SW wave vector. The pumped currents scale linearly with the frequency of the SW in experimentally relevant GHz–THz range. In contrast, recent experiments on magnonic charge pumping [7,24] were interpreted by invoking nonzero SO coupling in the band structure (alternatively, one could invoke magnetic or SO impurities [57]) to introduce misalignment between nonequilibrium electronic spin density and its 'adiabatic direction' defined by Eq. (13). This adds nonadiabatic contribution [51,52,56] to the spin motive force formula which describes charge pumping by time-dependent noncoplanar and noncollinear magnetic textures. Although SW is an example of such texture, standard purely adiabatic spin motive force formula [Eq. (7)] predicts zero pumped charge current [Sec. III B]. Thus our prediction highlights the importance of *time-retardation effects* [33,66,67], where conduction electron spin is always somewhat behind the 'adiabatic direction' that would instantaneously follow classical localized magnetic moments. The retardation is visualized by plotting the *nonadiabaticity angle* between the true and 'adiabatic direction' for conduction electron spin and classical localized magnetic moment, both in the absence [Fig. 5(e)] and in the presence [Fig. 5(f)] of SO coupling in the band structure. When dc spin-polarized charge current is injected into the ferromagnet, electrons interact with SW in such a way that the outflowing charge and spin current are changed both by the scattering off time-dependent potential generated by the SW and superposition with the currents pumped by the SW itself. Using Lorentzian voltage pulse to excite *spin-polarized leviton* out of the Fermi sea, which carries one electron charge with no accompanying electron-hole pairs and behaves as solitonlike quasiparticle, we also reveal how a *single* electron scatters from a *single* SW.

ACKNOWLEDGMENTS

We thank K. Belashchenko and Y. Tserkovnyak for illuminating discussions. This research was supported in part by the U.S. National Science Foundation (NSF) under Grant No. ECCS-1922689. It was finalized during *Spin and Heat Transport in Quantum and Topological Materials* program at KITP Santa Barbara, which is supported under NSF Grant No. PHY-1748958.

[1] S.-K. Kim, Micromagnetic computer simulations of spin waves in nanometre-scale patterned magnetic elements, J. Phys. D: Appl. Phys. **43**, 264004 (2010).

[2] R. F. L. Evans, W. J. Fan, P. Chureemart, T. A. Ostler, M. O. A. Ellis, and R. W. Chantrell, Atomistic spin model simulations of magnetic nanomaterials, J. Phys.: Condens. Matter **26**, 103202 (2014).

[3] B. Jungfleisch, W. Zhang, and A. Hoffmann, Perspectives of antiferromagnetic spintronics, Phys. Lett. A **382**, 865 (2018).

[4] C. P. Hofmann, Spontaneous magnetization of an ideal ferromagnet: Beyond Dyson's analysis, Phys. Rev. B **84**, 064414 (2011).

[5] P. E. Zil'berman, A. G. Terniryazev, and M. P. Tikhornirova, Excitation and propagation of exchange spin waves in films of yttrium iron garnet, JETP **81**, 151 (1995).

[6] V. E. Demidov, U.-H. Hansen, and S. O. Demokritov, Spin-Wave Eigenmodes of a Saturated Magnetic Square at Different Precession Angles, Phys. Rev. Lett. **98**, 157203 (2007).

[7] M. Evelt, H. Ochoa, O. Dzyapko, V. E. Demidov, A. Yurgens, J. Sun, Y. Tserkovnyak, V. Bessonov, A. B. Rinkevich, and S. O. Demokritov, Chiral charge pumping in graphene deposited on a magnetic insulator, Phys. Rev. B **95**, 024408 (2017).

[8] S. Woo, T. Delaney, and G. S. D. Beach, Magnetic domain wall depinning assisted by spin wave bursts, Nat. Phys. **13**, 448 (2017).

[9] C. Tzschaschel, K. Otani, R. Iida, T. Shimura, H. Ueda, S. Günther, M. Fiebig, and T. Satoh, Ultrafast optical excitation of coherent magnons in antiferromagnetic NiO, Phys. Rev. B **95**, 174407 (2017).

[10] C. W. Sandweg, Y. Kajiwara, A. V. Chumak, A. A. Serga, V. I. Vasyuchka, M. B. Jungfleisch, E. Saitoh, and B. Hillebrands, Spin Pumping by Parametrically Excited Exchange Magnons, Phys. Rev. Lett. **106**, 216601 (2011).

[11] B. Raquet, M. Viret, E. Sondergard, O. Cespedes, and R. Mamy, Electron-magnon scattering and magnetic resistivity in 3d ferromagnets, Phys. Rev. B **66**, 024433 (2002).

[12] A. A. Starikov, Y. Liu, Z. Yuan, and P. J. Kelly, Calculating the transport properties of magnetic materials from first principles including thermal and alloy disorder, noncollinearity, and spin-orbit coupling, Phys. Rev. B **97**, 214415 (2018).

[13] E. Carpene, E. Mancini, C. Dallera, M. Brenna, E. Puppin, and S. De Silvestri, Dynamics of electron-magnon interaction and ultrafast demagnetization in thin iron films, Phys. Rev. B **78**, 174422 (2008).

[14] V. Drewello, J. Schmalhorst, A. Thomas, and G. Reiss, Evidence for strong magnon contribution to the TMR temperature dependence in MgO based tunnel junctions, Phys. Rev. B **77**, 014440 (2008).

[15] F. Mahfouzi and B. K. Nikolić, Signatures of electron-magnon interaction in charge and spin currents through magnetic tunnel

junctions: A nonequilibrium many-body perturbation theory approach, Phys. Rev. B **90**, 045115 (2014).

[16] J. C. Slonczewski and J. Z. Sun, Theory of voltage-driven current and torque in magnetic tunnel junctions, J. Magn. Magn. Mater. **310**, 169 (2007).

[17] T. Balashov, A. F. Takács, M. Däne, A. Ernst, P. Bruno, and W. Wulfhekel, Inelastic electron-magnon interaction and spin transfer torque, Phys. Rev. B **78**, 174404 (2008).

[18] Y. Wang, D. Zhu, Y. Yang, K. Lee, R. Mishra, G. Go, S.-H. Oh, D.-H. Kim, K. Cai, E. Liu, S. D. Pollard, S. Shi, J. Lee, K. Leong Teo, Y. Wu, K.-J. Lee, and H. Yang, Magnetization switching by magnon-mediated spin torque through an antiferromagnetic insulator, Science **366**, 1125 (2019).

[19] Y. Cheng, W. Wang, and S. Zhang, Amplification of spin-transfer torque in magnetic tunnel junctions with an antiferromagnetic barrier, Phys. Rev. B **99**, 104417 (2019).

[20] N. Okuma and K. Nomura, Microscopic derivation of magnon spin current in a topological insulator/ferromagnet heterostructure, Phys. Rev. B **95**, 115403 (2017).

[21] Y. Kajiwara, K. Harii, S. Takahashi, J. Ohe, K. Uchida, M. Mizuguchi, H. Umezawa, H. Kawai, K. Ando, K. Takanashi, S. Maekawa and E. Saitoh, Transmission of electrical signals by spin-wave interconversion in a magnetic insulator, Nature (London) **464**, 262 (2010).

[22] J. Zheng, S. Bender, J. Armaitis, R. E. Troncoso, and R. A. Duine, Green's function formalism for spin transport in metal-insulator-metal heterostructures, Phys. Rev. B **96**, 174422 (2017).

[23] K. Uchida, J. Xiao, H. Adachi, J. Ohe, S. Takahashi, J. Ieda, T. Ota, Y. Kajiwara, H. Umezawa, H. Kawai, G. E. W. Bauer, S. Maekawa and E. Saitoh, Spin Seebeck insulator, Nat. Mater. **9**, 894 (2010).

[24] C. Ciccarelli, K. M. D. Hals, A. Irvine, V. Novak, Y. Tserkovnyak, H. Kurebayashi, A. Brataas, and A. Ferguson, Magnonic charge pumping via spin-orbit coupling, Nat. Nanotechnol. **10**, 50 (2014).

[25] G. Stefanucci and R. van Leeuwen, *Nonequilibrium Many-Body Theory of Quantum Systems: A Modern Introduction* (Cambridge University Press, Cambridge, 2013).

[26] M. N. Kiselev and R. Oppermann, Schwinger-Keldysh Semionic Approach for Quantum Spin Systems, Phys. Rev. Lett. **85**, 5631 (2000).

[27] H. Mera, T. G. Pedersen, B. K. Nikolić, Hypergeometric resummation of self-consistent sunset diagrams for steady-state electron-boson quantum many-body systems out of equilibrium, Phys. Rev. B **94**, 165429 (2016).

[28] J. Gukelberger, L. Huang, and P. Werner, On the dangers of partial diagrammatic summations: Benchmarks for the two-dimensional Hubbard model in the weak-coupling regime, Phys. Rev. B **91**, 235114 (2015).

[29] A. Spinelli, B. Bryant, F. Delgado, J. Fernández-Rossier, and A. F. Otte, Imaging of spin waves in atomically designed nanomagnets, Nat. Mater. **10**, 782 (2014).

[30] D. Ivanov, H. Lee, and L. Levitov, Coherent states of alternating current, Phys. Rev. B **56**, 6839 (1997).

[31] J. Keeling, I. Klich, and L. Levitov, Minimal Excitation States of Electrons in One-Dimensional Wires, Phys. Rev. Lett. **97**, 116403 (2006).

[32] M. D. Petrović, B. S. Popescu, U. Bajpai, P. Plecháč, and B. K. Nikolić, Spin and Charge Pumping by a Steady or Pulse-Current-Driven Magnetic Domain Wall: A Self-Consistent Multiscale Time-Dependent Quantum-Classical Hybrid Approach, Phys. Rev. Applied **10**, 054038 (2018).

[33] U. Bajpai and B. K. Nikolić, Time-retarded damping and magnetic inertia in the Landau-Lifshitz-Gilbert equation self-consistently coupled to electronictime-dependent nonequilibrium Green functions, Phys. Rev. B **99**, 134409 (2019).

[34] M. D. Petrović, P. Plecháč, and B. K. Nikolić, Annihilation of topological solitons in magnetism: How domain walls collide and vanish to burst spin waves and pump electronic spin current of broadband frequencies, arXiv:1908.03194.

[35] E. V. Boström and C. Verdozzi, Steering magnetic skyrmions with currents: A nonequilibrium Green's functions approach, Phys. Status Solidi B **256**, 1800590 (2019).

[36] B. Gaury, J. Weston, M. Santin, M. Houzet, C. Groth, and X. Waintal, Numerical simulations of time-resolved quantum electronics, Phys. Rep. **534**, 1 (2014).

[37] R. Wieser, Description of a dissipative quantum spin dynamics with a Landau-Lifshitz-Gilbert like damping and complete derivation of the classical Landau-Lifshitz equation, Eur. Phys. J. B **88**, 77 (2015).

[38] P. Mondal, U. Bajpai, M. D. Petrović, P. P. Plecháč, and B. K. Nikolić, Quantum spin-transfer torque induced nonclassical magnetization dynamics and electron-magnetization entanglement, Phys. Rev. B **99**, 094431 (2019).

[39] Y. Tserkovnyak, A. Brataas, G. E. W. Bauer, and B. I. Halperin, Nonlocal magnetization dynamics in ferromagnetic heterostructures, Rev. Mod. Phys. **77**, 1375 (2005).

[40] R. L. Cooper and E. A. Uehling, Ferromagnetic resonance and spin diffusion in supermalloy, Phys. Rev. **164**, 662 (1967).

[41] B. Popescu and A. Croy, Efficient auxiliary-mode approach for time-dependent nanoelectronics, New J. Phys. **18**, 093044 (2016).

[42] U. Bajpai, B. S. Popescu, P. Plecháč, B. K. Nikolić, L. E. F. Foa Torres, H. Ishizuka, and N. Nagaosa, Spatio-temporal dynamics of shift current quantum pumping by femtosecond light pulse, J. Phys.: Mater. **2**, 025004 (2019).

[43] S.-H. Chen, C.-R. Chang, J. Q. Xiao, and B. K. Nikolić, Phys. Rev. B **79**, 054424 (2009).

[44] F. Mahfouzi, J. Fabian, N. Nagaosa, and B. K. Nikolić, Charge pumping by magnetization dynamics in magnetic and semimagnetic tunnel junctions with interfacial Rashba or bulk extrinsic spin-orbit coupling, Phys. Rev. B **85**, 054406 (2012).

[45] K. Dolui, U. Bajpai, and B. K. Nikolić, Effective spin-mixing conductance of topological-insulator/ferromagnet and heavy-metal/ferromagnet spin-orbit-coupled interfaces: A first-principles Floquet-nonequilibrium-Green-function approach, arXiv:1905.01299.

[46] G. E. Bauer and Y. Tserkovnyak, Viewpoint: spin-magnon transmutation, Physics **4**, 40 (2011).

[47] A. Hallal, F. Ibrahim, H. X. Yang, S. Roche, and M. Chshiev, Tailoring magnetic insulator proximity effects in graphene: First-principles calculations, 2D Mater. **4**, 025074 (2017).

[48] G. E. Volovik, Linear momentum in ferromagnets, J. Phys. C: Solid State Phys. **20**, L83 (1987).

[49] S. E. Barnes and S. Maekawa, Generalization of Faraday's Law to Include Nonconservative Spin Forces, Phys. Rev. Lett. **98**, 246601 (2007).

[50] R. A. Duine, Spin pumping by a field-driven domain wall, Phys. Rev. B **77**, 014409 (2008).

[51] R. A. Duine, Effects of nonadiabaticity on the voltage generated by a moving domain wall, Phys. Rev. B **79**, 014407 (2009).
[52] Y. Tserkovnyak and M. Mecklenburg, Electron transport driven by nonequilibrium magnetic textures, Phys. Rev. B **77**, 134407 (2008).
[53] S. Zhang and S. S.-L. Zhang, Generalization of the Landau-Lifshitz-Gilbert Equation for Conducting Ferromagnets, Phys. Rev. Lett. **102**, 086601 (2009).
[54] Q. Niu and L. Kleinman, Spin-Wave Dynamics in Real Crystals, Phys. Rev. Lett. **80**, 2205 (1998).
[55] C. Stahl and M. Potthoff, Anomalous Spin Precession Under a Geometrical Torque, Phys. Rev. Lett. **119**, 227203 (2017).
[56] G. Tatara, Effective gauge field theory of spintronics, Physica E **106**, 208 (2019).
[57] H. Kohno, G. Tatara, and J. Shibata, Microscopic calculation of spin torques in disordered ferromagnets, J. Phys. Soc. Jpn. **75**, 113706 (2006).
[58] M. Milletarì, M. Offidani, A. Ferreira, and R. Raimondi, Covariant Conservation Laws and The Spin Hall Effect in Dirac-Rashba Systems, Phys. Rev. Lett. **119**, 246801 (2017).
[59] K. Zollner, M. D. Petrović, K. Dolui, P. Plecháč, B. K. Nikolić, and J. Fabian, Purely interfacial and highly tunable by gate or disorder spin-orbit torque in graphene doubly proximitized by two-dimensional ferromagnet $Cr_2Ge_2Te_6$ and monolayer WS_2, arXiv:1910.08072.
[60] A. Manchon, H. C. Koo, J. Nitta, S. M. Frolov and R. A. Duine, New perspectives for Rashba spin–orbit coupling, Nat. Mater. **14**, 871 (2015).
[61] A. Brataas, Y. Tserkovnyak, and G. E. W. Bauer, Magnetization dissipation in ferromagnets from scattering theory, Phys. Rev. B **84**, 054416 (2011).
[62] T. Taniguchi, K.-J. Kim, T. Tono, T. Moriyama, Y. Nakatani, and T. Ono, Precise control of magnetic domain wall displacement by a nanosecond current pulse in Co/Ni nanowires, Appl. Phys. Express **8**, 073008 (2015).
[63] N. Bode, L. Arrachea, G. S. Lozano, T. S. Nunner and F. von Oppen, Current-induced switching in transport through anisotropic magnetic molecules, Phys. Rev. B. **85**, 115440 (2012).
[64] F. Mahfouzi, B. K. Nikolić, and N. Kioussis, Antidamping spin-orbit torque driven by spin-flip reflection mechanism on the surface of a topological insulator: A time-dependent nonequilibrium Green function approach, Phys. Rev. B **93**, 115419 (2016).
[65] D. Ralph and M. Stiles, Spin transfer torques, J. Magn. Mater. **320**, 1190 (2008).
[66] M. Sayad and M. Potthoff, Spin dynamics and relaxation in the classical-spin Kondo-impurity model beyond the Landau-Lifschitz-Gilbert equation, New J. Phys. **17**, 113058 (2015).
[67] H. M. Hurst, Victor Galitski, and Tero T. Heikkilä, Electron-induced massive dynamics of magnetic domain walls, Phys. Rev. B **101**, 054407 (2020).
[68] V. Kamberský, Spin-orbital Gilbert damping in common magnetic metals, Phys. Rev. B **76**, 134416 (2007).
[69] K. Gilmore, Y. U. Idzerda, and M. D. Stiles, Identification of the Dominant Precession-Damping Mechanism in Fe, Co, and Ni by First-Principles Calculations, Phys. Rev. Lett. **99**, 027204 (2007).
[70] M. Moskalets and M. Büttiker, Floquet scattering theory of quantum pump, Phys. Rev. B **66**, 205320 (2002).
[71] L. E. F. Foa Torres, Mono-parametric quantum charge pumping: Interplay between spatial interference and photon-assisted tunneling, Phys. Rev. B **72**, 245339 (2005).
[72] J. Dubois, T. Jullien, F. Portier, P. Roche, A. Cavanna, Y. Jin, W. Wegscheider, P. Roulleau, and D. Glattli, Minimal-excitation states for electron quantum optics using levitons, Nature (London) **502**, 659 (2013).
[73] M. Moskalets, Fractionally Charged Zero-Energy Single-Particle Excitations in a Driven Fermi Sea, Phys. Rev. Lett. **117**, 046801 (2016).
[74] B. Gaury and X. Waintal, A computational approach to quantum noise in time-dependent nanoelectronic devices, Physica E **75**, 72 (2016).